Thermodynamic Properties of HFC-338mccq, $CF_3CF_2CF_2CH_2F$, 1,1,1,2,2,3,3,4-Octafluorobutane†

D. R. Defibaugh,* E. Carrillo-Nava, J. J. Hurly, M. R. Moldover, J. W. Schmidt, and L. A. Weber

Physical and Chemical Properties Division, Chemical Science & Technology Laboratory, National Institute of Standards and Technology, Gaithersburg, Maryland 20899

We report the thermodynamic properties of 1,1,1,2,2,3,3,4-octafluorobutane, which has been designated as HFC-338mccq by the refrigeration industry. The measurements span the temperature and pressure ranges encountered in thermal machinery. The properties measured include the vapor pressure, the density of the compressed liquid, the refractive index of both the saturated liquid and the saturated vapor, the critical temperature, the capillary rise, and the speed of sound in the vapor phase. These data were used to determine the ideal gas heat capacity, the saturated liquid and vapor densities, the surface tension, the virial equation of state for the vapor phase, and estimates of the critical pressure and density. A Carnahan−Starling−DeSantis equation of state was deduced from the measured fluid properties.

Introduction

Evidence linking the depletion of the earth's protective ozone layer to the release into the environment of anthropogenic chlorine-containing compounds continues to mount. In 1987 the international community agreed under the Montreal Protocol (1987) to phase out the manufacture and/or use of chlorofluorocarbons (CFC) and hydrochlorofluorocarbons (HCFC) as working fluids in thermal machinery. In an effort to contribute to the Montreal Protocol, many laboratories have characterized the thermodynamic properties of possible replacement compounds. Here we report our results for one such fluid, identified as HFC-338mccq (1,1,1,2,2,3,3,4-octafluorobutane). HFC-338mccq is being considered as a component of an azeotropic mixture with HFC-245ca (1,1,2,2,3-pentafluoropropane). The mixture is less flammable than pure HFC-245ca and it is a possible replacement for CFC-11 (trichlorofluoromethane).

The present measurements of the thermodynamic properties of HFC-338mccq span the temperature range from 243 K to the critical temperature T_c = 431.95 K. The measurements were performed with specialized apparatus that have long histories of yielding consistent, accurate data. The vapor pressure was measured using a comparative ebulliometer. The vapor pressure data span the pressure range 16 kPa to 500 kPa, corresponding to the temperature range 260 K to 352 K. Compressed liquid densities were measured with a vibrating tube densimeter on 29 isotherms ranging from 243 K to 371 K at pressures from 500 kPa to 6500 kPa. The compressed liquid density data were extrapolated on their isotherms to the vapor pressure curve to obtain saturated liquid densities. The refractive indices of the saturated liquid and vapor were measured simultaneously with the capillary rise in an optical cell in the temperature range 295 K to 430 K. These data yielded the critical temperature and the temperature-dependent capillary length. The Lorentz−Lorenz constant was determined by comparing the refractive index of the liquid phase with the liquid density. The refractive index data were combined with the Lorentz−Lorenz constant to deduce the critical density and the densities of the saturated liquid and vapor near the critical temperature. The saturated vapor and liquid density data were combined with the capillary rise to calculate the surface tension. The speed of sound in the vapor phase was measured using a highly accurate resonance technique on six isotherms between 300 K and 400 K and at pressures from 40 kPa to 400 kPa. From the speed-of-sound data, the ideal gas heat capacity and the virial equation of state of the vapor phase were deduced. Finally, the vapor pressure and the saturated liquid densities were used to determine the parameters of a Carnahan−Starling−DeSantis (CSD) equation of state. This equation reproduces the saturated liquid densities and the vapor pressure within ±0.4% from 280 K to 410 K.

† Brand names and commercial sources of materials and instruments, when noted, are given for scientific completeness. Such information does not constitute a recommendation by the National Institute of Standards and Technology nor does it suggest that these products or instruments are the best for the described application.

Table 1. Retention Times of Impurities in the HFC-338mccq Sample

	retention time/min	integrated % area
air	0.637	0.0201
impurity no. 1	0.783	0.0202
impurity no. 2	0.917	0.0454
impurity no. 3	1.048	0.1412
impurity no. 4	2.573	0.0088
impurity no. 5	3.642	0.0027
impurity no. 6	9.283	0.0705
HFC-318mccq	11.527	99.691

Materials, Apparatus, and Procedure

Sample Purity. The manufacturer of HFC-338mccq, PCR Inc., claimed that the sample had a mass fraction purity of 99.9%. No information was provided about the identity of the impurities within the sample. A gas chromatograph (GC) utilizing a thermal conductivity detector and Carbopak 5% Fluorocol column at 45 °C was used to validate the manufacturer's purity claims. We found the sample to have a 99.7% area ratio purity for HFC-338mccq with the remaining 0.3% containing air and six other unknown impurities. The retention times and integrated areas for each impurity are listed in Table 1.

The sample was analyzed for water content by a Karl Fisher titration. The titration yielded a 21 μL/L water concentration. An unsuccessful attempt was made to purify the sample using a preparative gas chromatograph. The preparative GC was equipped with two 3-m columns containing PoraPlot-Q packing material.

S0021-9568(96)00313-5 This article not subject to U.S. Copyright. Published 1997 by the American Chemical Society

Table 2. Refractive Index

T/K	n_v	n_l	T/K	n_v	n_l
431.829	1.0805	1.1058	424.383	1.046	1.1429
431.731	1.0783	1.108	422.271	1.0425	1.1481
431.618	1.0767	1.1096	416.709	1.0353	1.1585
431.472	1.0746	1.1116	408.085	1.0272	1.1704
431.191	1.0718	1.1144	398.504	1.0208	1.1815
430.941	1.0691	1.1173	388.239	1.0164	1.1918
430.713	1.0675	1.1189	373.256	1.0114	1.2044
430.039	1.0634	1.1233	353.371	1.0069	1.2182
429.531	1.0608	1.1261	333.025	1.0043	1.2313
429.017	1.0588	1.1289	312.964	1.0028	1.2423
428.066	1.0553	1.1325	296.582	1.0016	1.2513
426.941	1.0521	1.1361			

We did remove volatile impurities from the sample by repeated freeze (at 77 K)−pump−thaw cycles before loading the sample into each apparatus. Assuming that the air was removed by degassing, the purity for HFC-338mccq studied in this work was approximately 99.7% (by GC area ratio).

Refractive Index and Capillary Rise. The apparatus used to measure the refractive indices and the capillary rise has been thoroughly described elsewhere (Chae et al. (1990)); only a brief description is given here. The cell was constructed of stainless steel, sapphire, and gold. The body of the cell was a hollow stainless steel cylinder 2.54 cm long with an internal volume of 6.5 cm^3. The cylinder was closed on both ends with sapphire windows sealed with gold O-rings. A fused silica prism and four capillary tubes with radii of (0.574 ± 0.001) mm, (0.320 ± 0.001) mm, (0.276 ± 0.001) mm, and (0.0148 ± 0.001) mm were mounted inside the cell. The sapphire windows allowed a cathetometer to measure the differences in the capillary rise between pairs of capillaries. The capillary length was deduced from these differences and from prior measurements of the bore radii of the capillaries following Lane's procedure (1973). HFC-338mccq appears to completely wet the capillaries, and the data were analyzed accordingly. The differential technique allows one to analyze the data without making the approximation that the capillary rise was much larger than the radii of the capillaries. Consistent results were obtained with different pairs of capillaries.

The sapphire windows on this cell allowed laser light (633 nm) to pass through the cell and the prism inside the cell. The apex of the prism in the cell was illuminated with the collimated laser beam, and it refracted the beam into two beams that diverged from each other at an angle that depended upon the difference between the refractive index of the liquid (or vapor) phase and that of the silica prism. The uncertainty in the angle measurement was 0.001 radian and that led to an overall standard uncertainty of $\delta n = 0.0005$ (1σ) in the refractive indexes of the fluid.

The cell was initially flushed several times with small aliquots of degassed HFC-338mccq sample. The cell was then loaded and immersed in a thermostated oil bath. The bath temperature was monitored with a platinum resistance thermometer with an accuracy of ±0.02 K. Temperature equilibrium between the oil bath and the cell generally occurred within 10 min; however, 1 h was allowed to elapse between measurements. The bath temperature was increased in 20 K intervals and the refractive index (Table 2) and capillary rise (Table 3) were measured at each step. This increase in temperature continued until the critical temperature was exceeded. The temperature was then raised and lowered in successively smaller increments until the critical temperature of this sample was determined to be 431.95 K with a precision of ±0.02 K. The uncertainty in the critical temperature resulting from the unknown impurities is much larger.

Table 3. Capillary Rise

T/K	$(a/\text{mm})^2$	T/K	$(a/\text{mm})^2$
430.713	0.12	408.085	0.323
430.039	0.021	398.504	0.445
429.531	0.027	388.239	0.567
429.017	0.038	373.256	0.755
428.066	0.051	353.371	0.995
426.941	0.067	333.025	1.241
424.383	0.106	312.964	1.467
422.271	0.133	296.582	1.643
416.709	0.211		

Vapor Pressure. Vapor pressure measurements were made using a comparative ebulliometer. A detailed description of the ebulliometer apparatus has been given in previous publications (Goodwin et al. (1992a), Weber (1992), Goodwin et al. (1992b), Weber and Goodwin (1993)); here we provide only a brief overview of the equipment and methodology. The comparative ebulliometer consisted of two boilers connected to a common manifold, all constructed out of stainless steel. One boiler was loaded with HFC-338mccq and the other boiler was loaded with a reference fluid, R134a (1,1,1,2-tetrafluoroethane). The common manifold allowed measurement of the condensation temperature of HFC-338mccq and that of the reference fluid at a single known pressure. The pressure was known from the well-characterized vapor pressure−temperature curve of R134a (Goodwin et al. (1992a)).

Condensation temperatures within the boilers were measured using platinum resistance thermometers (PRTs). The PRTs were calibrated on the ITS-90 scale, and their accuracy and stability were verified using a triple-point-of-water cell.

Initially, one boiler was loaded with 50 cm^3 of HFC-338mccq and the other boiler was loaded with 50 cm^3 of R134a. This was done with the ebulliometer evacuated to a pressure below 1 Pa and cooled to 273 K. The two boilers and the common manifold were then pressurized with helium gas to the desired pressure. Then, the boilers were gradually heated until the two fluids began to boil. The ebulliometer was determined to be in a steady state when the temperature readings from both PRTs were stable within ±0.01 K for 10 min. Then the temperature was recorded. The pressure was obtained from the vapor pressure correlation of R134a (Goodwin et al. (1992a)). After recording a series of pressure−temperature measurements at equilibrium, the pressure of the helium in the apparatus was increased. More heat was then gradually applied under the boilers until equilibrium was re-established at the higher pressure and the data collection resumed.

Compressed Liquid Density. A commercially manufactured vibrating tube densimeter, Anton-PAAR model DPR412Y, was used to measure compressed liquid densities. The calibration of this apparatus has been discussed elsewhere (Defibaugh and Morrison (1990), Defibaugh and Moldover (1997)). Defibaugh and Moldover (1997) provide extensive evidence to show that the relative expanded uncertainty in the measured densities is less than 0.05%, except in the critical region. The densimeter was maintained within an insulated air bath. A thermostated water/ethylene glycol mixture was circulated through a jacket surrounding the densimeter and through a heat exchanger within the air bath. A platinum resistance thermometer was used to monitor the temperature of the water exiting the jacket surrounding the densimeter. The uncertainty in the temperature (ITS-90) measurements was ±0.01 K.

A manifold located outside the air bath contained mercury reservoirs and a mercury-filled manometer/separator. The mercury separator isolated the sample from argon used

to control the pressure of the sample. A glass capillary in the separator allowed observation of the mercury level. The pressure of the system was maintained 200 kPa above the saturated vapor pressure of HFC-338mccq throughout the entire temperature range of the experiment. The pressure of the argon was measured with an uncertainty of ±0.5 kPa with a quartz pressure transducer.

Prior to loading the densimeter, it was rinsed with ethanol and then acetone to remove residue from previous experiments. The apparatus was then evacuated and cooled to 273 K. Mercury was drawn into the reservoirs and into the manometer/separator. Finally, refrigerant sample was condensed into the manifold and the vibrating tube. Once the apparatus was filled, compressed liquid densities for HFC-338mccq were measured.

Speed of Sound. The speed of sound in gaseous HFC-338mccq was measured using high-accuracy acoustic resonance techniques developed by our laboratory. A detailed description of both the apparatus and the acoustic model used to reduce the data has been given in previous publications (Gillis (1994), Gillis et al. (1991)). A brief summary is given here.

The speed of sound was determined from the acoustic resonances in the gas when it was confined within an all-metal cylindrical cavity. For several acoustic modes, the resonance frequencies and half-widths were determined by fitting the complex frequency response of the cavity in the vicinity of each mode. The resonance frequencies were corrected for the effects of viscous and thermal energy losses with a well-established acoustic model. The dimensions of the resonator as a function of temperature had been determined from resonance measurements when the cavity was filled with argon, a gas for which the thermophysical properties are accurately known.

Two electro-acoustic transducers (a source and a detector) in separate enclosures were located outside of the fluid bath at ambient temperature. Sound was transmitted between the transducers and the resonator through acoustic waveguides filled with argon. Two thin metal diaphragms, mounted flush with the interior of the resonator, separated the argon from the sample gas within the resonator. The argon pressure in the waveguides and in the transducer enclosures was maintained equal to the sample pressure in the resonator so that the stress on the diaphragms was a minimum. A 13 kPa full-scale differential pressure transducer was used to indicate the pressure difference between the argon and the sample gas. The argon pressure was measured with a quartz Bourdon-tube pressure gauge. This gauge had been calibrated with a dead weight piston gauge referenced to a calibrated barometer and was found to have an uncertainty of $\sigma_p = ((100 \times 10^{-6}P)^2 + (30\ \text{Pa})^2)^{1/2}$. The differential pressure transducer and the gas manifold were maintained near 350 K to prevent condensation of the sample at high pressures.

The resonator was in a thermostatically controlled bath with millikelvin stability. A platinum resistance thermometer and a high-precision dc multimeter were used to measure the temperature on ITS-90.

The speed of sound was measured on isotherms starting at the highest pressure achievable with the limited volume of sample available. The resonance frequencies at each state were measured after the temperature and pressure had stabilized. To reduce the sample pressure, a portion of the sample was removed from the resonator and collected in a cold trap at 77 K. This process was repeated down to a pressure of approximately 50 kPa, where the decrease in the signal to noise ratio prevented further measurements. The data acquisition and instrument control for each isotherm were fully automated; however, the sample was loaded into the resonator manually.

Our resonance technique yields sound speeds with random uncertainties of about 0.01%, corresponding to two standard deviations (2σ). As discussed below, the constant-pressure ideal gas heat capacity $C_p^\circ(T)$ is typically obtained from the zero pressure limit of the speed of sound with a 2σ uncertainty of 0.1% or less. However, for HFC-338mccq, a much larger uncertainty in $C_p^\circ(T)$ results from the uncertainty of the sample's average molecular weight because of the unidentified impurities. Uncertainties as large as 0.5% × $C_p^\circ(T)$ could result from the 0.3% impurity within this sample (Gillis (1994)).

Results

Refractive Index and Capillary Rise. The refractive indices for HFC-338mccq are listed in Table 2. These data were fit with the following equations:

$$n_l - n_v = 0.3432\tau^{0.325}(1 + 0.4225\tau^{0.5} - 0.575\tau) \quad (1)$$

$$n_l + n_v = 2.1862(1 + 0.0984\tau) \quad (2)$$

where $\tau = (T_c - T)/T_c$ and the subscripts l and v refer to the saturated liquid and vapor, respectively. The value of T_c determined for the sample by eq 1 was (431.95 ± 0.02) K and the root mean square (rms) standard deviation of the refractive index data from eqs 1 and 2 was 0.0004. The uncertainty in T_c from the unknown impurities is undoubtedly much larger than 0.02 K.

We used the Lorentz−Lorenz relation

$$\frac{n^2 - 1}{n^2 + 2} = k\rho \quad (3)$$

to deduce densities from the refractive index data. The value $k = 0.1062\ \text{cm}^3\cdot\text{g}^{-1}$ for the Lorentz−Lorenz constant that appears in eq 3 was determined by combining the value of n_l from eqs 1 and 2 with the value $\rho_l = 1274.6\ \text{kg}\cdot\text{m}^{-3}$ for the saturated liquid density at 362.58 K. The saturated liquid density at 362.58 K was obtained by extrapolating the desimeter data to the saturation boundary. Once k was determined, eq 3 was used to estimate ρ_l and ρ_v from the tabulated values of n_l and n_v.

The estimated standard uncertainty in the refractive index $\delta n = 0.0005$ with a coverage factor of 1 leads, through eq 3, to an uncertainty in the density $\delta\rho = 7.5\ \text{kg}\cdot\text{m}^{-3}$. The fractional uncertainty in the density, $\delta\rho/\rho = \delta n/(n - 1)$, diverges as $\rho \to 0$ and $n \to 1$.

The estimated values of ρ_l and ρ_v were fit by the equations

$$(\rho_l - \rho_v)/\text{kg}\cdot\text{m}^{-3} = 2072.1\tau^{0.325}(1 + 0.4396\tau^{0.5} - 0.664\tau) \quad (4)$$

$$(\rho_l + \rho_v)/(2\ \text{kg}\cdot\text{m}^{-3}) = 572.4(1 + 1.001\tau) \quad (5)$$

Equations 4 and 5 are valid over the temperature range 295 K to 430 K and are particularly useful in the vicinity of the critical point. The coefficient 572.4 kg/m^3 in eq 5 is the critical density ρ_c. We have assumed that the Lorentz−Lorenz "constant" k is indeed a constant because the temperature and density dependencies of k have not been determined for HFC-338mccq. Experience with several other fluids (Chae et al. (1990)), shows that this assumption led to a *worst-case* error in the coexisting densities of 0.8% for water. This corresponded to approximately 2.2% of ρ_c for water. However, as shown below, our independent

determination of ρ_c for HFC-338mccq led to a value of ρ_c that is only 0.07% smaller than the present value of ρ_c. Thus, we use the standard deviation ($1\sigma = 3.0$ kg·m^{-3}) of the fitted value of ρ_c as the measure of its uncertainty.

The surface tension of HFC-338mccq was deduced from measurements of the capillary rise in tubes of different diameters and the density differences given by eq 4 above. The square of the capillary length can be represented by

$$(a/\text{mm})^2 = 4.79\tau^{0.935}(1 - 0.106\tau) \quad (6)$$

The standard deviation of the capillary length data from eq 6 was [0.005 + 0.0003($T_c - T$)/K] mm^2. The capillary length data for HFC-338mccq are listed in Table 3. Equations 4 and 6 were used to compute the surface tension σ with the relation:

$$\sigma = a^2/[(\rho_l - \rho_v)2g] \quad (7)$$

where g is the acceleration due to gravity.

The values of the surface tension may be represented by

$$\sigma/\text{mN·m}^{-1} = 43.20\tau^{1.26}(1 + 1.378\tau^{0.5} - 1.81\tau) \quad (8)$$

Vapor Pressures. Vapor pressure data were measured in two runs on the same sample. Measurements were made at 35 temperatures between 260 K and 352 K. Pressures varied from 16 kPa to 500 kPa. Two of the data were deleted because they deviated from a fitting curve by more than 3 standard deviations. The results are given in Table 4. The first eight data of run 1 are separated in the table because they were suspected of being affected by impurities in the HFC-338mccq sample. They were not used to determine the vapor pressure curve.

The data set was fitted by the following vapor pressure equation:

$$\ln \frac{P}{P_c} = \frac{T_c}{T}[A_1\tau + A_2\tau^{1.5} + A_3\tau^{2.5} + A_4\tau^5] \quad (9)$$

$A_1 = -7.89876$ $\quad T_c = 431.95$ K
$A_2 = 1.65966$ $\quad P_c = 2725.7$ kPa
$A_3 = -3.02432$
$A_4 = -5.29214$

where P_c and T_c are critical parameters and $\tau = (1 - T/T_c)$. The critical temperature was fixed at 431.95 K from the refractive index data. Equation 9 yields a critical pressure of 2725.7 kPa with a standard deviation of 166 kPa. The relative standard deviation of the fit was 0.023% of the pressure.

Deviations of the data from eq 9 are shown in Figure 1. The first eight data that were not used in the correlation are given a different symbol. These data all show positive deviations; their average deviation is almost 3 times the standard deviation of the remaining data. Those deviations are readily explained by the presence of a declining concentration of a volatile impurity. The design of the ebulliometer is such that, as the sample boils, it slowly circulates through the boiler/condenser system. In this way, impurities are carried up into the condenser. Volatile impurities such as air, carbon dioxide, and nitrogen do not condense in the condenser; therefore they are not returned to the boiler. Any volatile impurity within the sample when first loaded into the ebulliometer will ultimately escape by diffusing into the pressurizing helium gas at the helium−vapor interface in the condenser. Slightly volatile impurities escape more slowly than very volatile impurities.

Table 4. Vapor Pressures of HFC-338mccq[a]

run 1		run 2	
T/K	P/kPa	T/K	P/kPa
289.374	65.120	259.569	15.895
291.181	70.098	260.726	16.911
292.892	75.086	261.826	17.930
294.508	80.046	263.837	19.920
296.047	85.086	265.752	21.975
297.520	90.130	268.265	24.965
298.933	95.202	271.982	29.952
300.282	100.110	275.232	34.946
		278.132	39.960
302.838	110.087	283.171	50.015
305.217	120.101	285.376	54.962
307.435	130.101	287.427	59.961
311.518	150.08	289.346	64.947
320.122	200.07	291.155	69.956
327.198	250.09	297.507	89.966
333.256	300.10	300.265	99.959
343.373	400.17		
351.722	500.35		

[a] The first eight data of run 1 were not used in the results, see text.

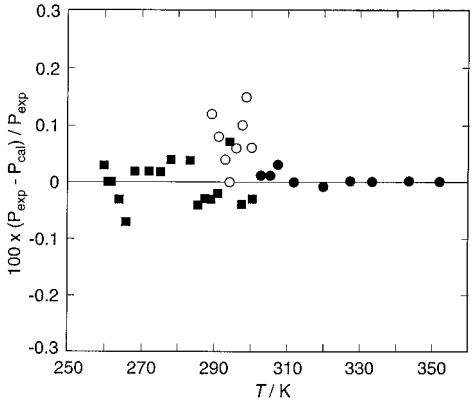

Figure 1. Vapor pressure deviations from eq 9: (○) data not used in fit; (■) run no. 1; (●) run no. 2.

In fact the sample itself also escapes slowly; however, the number of moles escaping is negligible compared to the total number of moles in the boiler. All of the impurities encountered in this HFC-338mccq had smaller retention times in the gas chromatograph than the sample itself, which indicates that the impurities are more volatile than HFC-338mccq. The longer the sample was studied in the ebulliometer, the purer the sample became.

Compressed Liquid Density. Compressed-liquid density measurements were made along isotherms between 243 K and 371 K at pressures from 500 kPa to 6500 kPa. The densities, listed in Table 5, range from 1.24 g·cm^{-3} to 1.66 g·cm^{-3}. The $P\rho T$ relation for the compressed liquid surface was represented by a polynomial function of temperature and pressure with the following form:

$$\rho/\text{g·cm}^{-3} = A_\rho(T) + B_\rho(T)P + C_\rho(T)P^2 \quad (10)$$

where

$$A_\rho(T) = \sum_{i=1}^{5} A_{\rho i}(T)^{i-1}$$

$$B_\rho(T)/\text{kPa} = \sum_{i=1}^{5} B_{\rho i}(T)^{i-1}$$

$$C_\rho(T)/\text{kPa}^2 = \sum_{i=1}^{5} C_{\rho i}(T)^{i-1}$$

Table 5. Compressed Liquid Densities of HFC-338mccq

T/K	*P*/MPa	ρ/g·cm^{-3}	*T*/K	*P*/MPa	ρ/g·cm^{-3}	*T*/K	*P*/MPa	ρ/g·cm^{-3}
243.314	0.1938	1.6468	242.338	0.3944	1.6499	242.356	0.9945	1.6510
242.356	1.4944	1.6521	242.358	1.9942	1.6531	242.367	2.4940	1.6540
242.377	2.9938	1.6550	242.368	3.4937	1.6560	242.367	3.9934	1.6570
242.377	4.4932	1.6580	242.347	4.9931	1.6590	242.345	5.4929	1.6600
242.355	5.9928	1.6609	242.388	6.4926	1.6617	248.729	0.1940	1.6325
248.077	0.3944	1.6346	248.092	0.9945	1.6359	248.098	1.4944	1.6369
248.106	1.9943	1.6380	248.118	2.4941	1.6390	248.113	2.9939	1.6401
248.100	3.4937	1.6412	248.111	3.9935	1.6422	248.107	4.4932	1.6432
248.109	4.9931	1.6443	248.115	5.4929	1.6453	248.109	5.9928	1.6463
248.121	6.4926	1.6473	252.462	0.1941	1.6225	251.937	0.3943	1.6243
251.938	0.9944	1.6257	251.939	1.4943	1.6268	251.949	1.9943	1.6279
251.955	2.4940	1.6290	251.956	2.9938	1.6301	251.967	3.4936	1.6312
251.967	3.9934	1.6323	251.960	4.4932	1.6334	251.950	4.9930	1.6345
251.951	5.4928	1.6355	251.960	5.9927	1.6365	251.957	6.4926	1.6376
257.230	0.1940	1.6096	256.719	0.3944	1.6115	256.731	0.9944	1.6129
256.734	1.4943	1.6141	256.765	1.9942	1.6152	256.777	2.4941	1.6164
256.732	2.9939	1.6177	256.741	3.4937	1.6188	256.767	3.9934	1.6199
256.775	4.4932	1.6210	256.775	4.9931	1.6221	256.791	5.4929	1.6232
256.788	5.9928	1.6243	256.797	6.4926	1.6253	260.209	0.1935	1.6016
259.675	0.3943	1.6035	259.686	0.9944	1.6050	259.671	1.4943	1.6063
259.677	1.9943	1.6075	259.677	2.4940	1.6087	259.681	2.9939	1.6099
259.669	3.4937	1.6111	259.656	3.9934	1.6123	259.679	4.4932	1.6134
259.685	4.9931	1.6145	259.686	5.4929	1.6157	259.683	5.9928	1.6168
259.689	6.4925	1.6180	264.915	0.1941	1.5887	264.511	0.3944	1.5904
264.673	0.9945	1.5916	264.722	1.4944	1.5927	264.739	1.9943	1.5939
264.753	2.4941	1.5952	264.760	2.9938	1.5964	264.764	3.4937	1.5977
264.766	3.9934	1.5989	264.793	4.4932	1.6001	264.807	4.9929	1.6013
264.818	5.4929	1.6025	264.810	5.9927	1.6037	264.827	6.4925	1.6048
269.625	0.1940	1.5758	269.641	0.3944	1.5763	269.636	0.9944	1.5780
269.632	1.4944	1.5794	269.637	1.9942	1.5808	269.636	2.4940	1.5821
269.632	2.9938	1.5834	269.647	3.4936	1.5847	269.641	3.9934	1.5861
269.636	4.4932	1.5874	269.646	2.9931	1.5887	269.657	5.4929	1.5899
269.654	5.9927	1.5912	269.663	6.4924	1.5924	272.511	0.1922	1.5678
272.588	0.3944	1.5682	272.575	0.9943	1.5700	272.573	1.4944	1.5714
272.588	0.3944	1.5682	272.575	0.9943	1.5700	272.573	1.4944	1.5714
272.577	1.9942	1.5728	272.588	2.4939	1.5742	272.586	2.9938	1.5755
272.597	3.4936	1.5769	272.519	3.9933	1.5784	272.542	4.4932	1.5797
272.503	4.9930	1.5812	272.519	5.4929	1.5824	272.532	5.9927	1.5837
272.530	6.4925	1.5850	275.347	0.1942	1.5599	274.948	0.3943	1.5617
275.056	0.9943	1.5632	275.072	1.4943	1.5646	275.075	1.9941	1.5660
275.078	2.4939	1.5675	275.078	2.9936	1.5689	275.083	3.4934	1.5703
275.098	3.9935	1.5716	275.088	4.4930	1.5730	275.093	4.9928	1.5744
275.093	5.4926	1.5758	275.095	5.9925	1.5771	275.102	6.4922	1.5784
278.732	0.1942	1.5504	278.891	0.3942	1.5506	278.923	0.9943	1.5524
278.918	1.4942	1.5540	278.920	1.9941	1.5555	278.892	2.4938	1.5570
278.891	2.9936	1.5585	278.922	3.4934	1.5600	278.908	3.9937	1.5615
278.913	4.4930	1.5629	278.911	4.9933	1.5643	278.935	5.4929	1.5656
278.927	5.9924	1.5670	278.920	6.4923	1.5684	283.667	0.1944	1.5365
283.797	0.3938	1.5367	283.792	0.9939	1.5387	283.801	1.4939	1.5403
283.827	1.9938	1.5418	283.831	2.4936	1.5434	283.812	2.9934	1.5450
283.812	3.4930	1.5466	283.838	3.9926	1.5481	283.883	4.4923	1.5495
283.867	4.9918	1.5510	283.821	5.4913	1.5526	283.785	5.9913	1.5542
283.788	6.4907	1.5556	288.595	0.1943	1.5224	288.722	0.3934	1.5226
288.729	0.9932	1.5247	288.728	1.4930	1.5265	288.726	1.9928	1.5282
288.726	2.4926	1.5299	288.734	2.9923	1.5315	288.736	3.4919	1.5331
288.737	3.9920	1.5348	288.759	4.4908	1.5363	288.772	4.9910	1.5379
288.743	5.4907	1.5395	288.745	5.9909	1.5411	288.734	6.4904	1.5426
293.547	0.1943	1.5080	293.689	0.3927	1.5082	293.703	0.9928	1.5104
293.656	1.4928	1.5124	293.704	1.9919	1.5141	293.616	2.4921	1.5161
293.558	2.9922	1.5181	293.487	3.4911	1.5200	293.399	3.9913	1.5221
293.445	4.4904	1.5237	293.505	4.9905	1.5252	293.509	5.4902	1.5269
293.501	5.9898	1.5285	293.524	6.4902	1.5300	298.565	0.1942	1.4931
298.563	0.3943	1.4939	303.643	0.2143	1.4780	303.645	0.3945	1.4788
308.582	0.2444	1.4631	308.566	0.3943	1.4638	313.475	0.2644	1.4480
313.472	0.3945	1.4486	298.428	0.4924	1.4948	298.356	0.9921	1.4969
298.379	1.4918	1.4988	298.342	1.9925	1.5009	298.332	2.4920	1.5028
298.437	4.4929	1.5098	298.410	4.9928	1.5117	298.412	5.4926	1.5134
298.421	5.9924	1.5151	298.420	6.4922	1.5168	303.431	0.5942	1.4803
303.397	0.9943	1.4821	303.454	1.4942	1.4840	303.484	1.9940	1.4859
303.492	2.4939	1.4879	303.468	2.9936	1.4900	303.447	3.4934	1.4920
303.464	3.9932	1.4939	303.422	4.4930	1.4959	303.414	4.9930	1.4979
303.434	5.4927	1.4997	303.391	5.9926	1.5016	303.379	6.4924	1.5034
308.280	0.6943	1.4661	308.221	0.9944	1.4676	308.259	1.4943	1.4607
308.287	1.9942	1.4718	308.256	2.4940	1.4741	308.283	2.9938	1.4761
308.287	3.4936	1.4782	308.301	3.9933	1.4802	308.285	4.4931	1.4823
308.290	4.9929	1.4843	308.294	5.4928	1.4862	308.301	5.9926	1.4881
308.316	6.4924	1.4900	313.178	0.6942	1.4511	313.176	0.9943	1.4525
313.210	1.4943	1.4548	313.190	1.9942	1.4572	313.200	2.4939	1.4595
313.201	2.9937	1.4617	313.185	3.4936	1.4640	313.227	3.9933	1.4660
313.238	4.4931	1.4681	313.218	4.9930	1.4703	313.309	5.4928	1.4721
313.257	5.9927	1.4743	313.275	6.4924	1.4763	318.445	0.3941	1.4330
318.442	0.9941	1.4361	318.439	1.4941	1.4387	318.442	1.9940	1.4412
318.441	2.4938	1.4436	318.440	2.9936	1.4461	318.436	3.4934	1.4485
318.437	3.9932	1.4508	318.438	4.4929	1.4531	318.438	4.9928	1.4553
318.440	5.4927	1.4575	318.440	5.9925	1.4597	318.440	6.4923	1.4618
323.301	0.3941	1.4172	323.304	0.9941	1.4206	323.306	1.4940	1.4233
323.311	1.9939	1.4260	323.309	2.4938	1.4287	323.307	2.9936	1.4313
323.310	3.4934	1.4338	323.313	3.9932	1.4363	323.333	4.4930	1.4386
323.331	4.9928	1.4410	323.333	5.4927	1.4434	323.333	5.9924	1.4457
323.333	6.4923	1.4480	328.205	0.3941	1.4009	328.206	0.9941	1.4046
328.204	1.4940	1.4075	328.204	1.9939	1.4104	328.204	2.4937	1.4133
328.209	2.9936	1.4160	328.208	3.4934	1.4187	328.206	3.9931	1.4214
328.206	4.4930	1.4240	328.208	4.9928	1.4265	328.207	5.4926	1.4290
328.209	5.9924	1.4315	328.207	6.4923	1.4339	333.060	0.4941	1.3851
333.061	0.9941	1.3883	333.058	1.4941	1.3915	333.061	1.9939	1.3946
333.058	2.4937	1.3977	333.062	2.9935	1.4006	333.060	3.4933	1.4035
333.058	3.9931	1.4063	333.060	4.4929	1.4091	333.060	4.9928	1.4118
333.061	5.4926	1.4145	333.058	5.9923	1.4171	333.059	6.4923	1.4197
338.062	0.4940	1.3676	338.061	0.9940	1.3711	338.062	1.4940	1.3746
338.060	1.9939	1.3780	338.062	2.4937	1.3812	338.062	2.9935	1.3844
338.058	3.4933	1.3875	338.060	3.9931	1.3906	338.060	4.4928	1.3935
338.058	4.9926	1.3965	338.060	5.4923	1.3993	338.060	5.9921	1.4021
338.062	6.4921	1.4048	343.029	0.5932	1.3505	343.032	0.9932	1.3536
343.030	1.4940	1.3573	343.031	1.9939	1.3610	343.033	2.4938	1.3645
343.031	2.9925	1.3680	343.030	3.4928	1.3713	343.030	3.9934	1.3746
343.026	4.4932	1.3778	343.028	4.9930	1.3809	343.035	5.4926	1.3839
343.030	5.9926	1.3869	343.032	6.4924	1.3898	347.965	0.5941	1.3322
347.967	0.9942	1.3356	347.970	1.4941	1.3397	347.968	1.9940	1.3437
347.971	2.4939	1.3475	347.974	2.9937	1.3512	347.973	3.4936	1.3548
347.971	3.9934	1.3584	347.976	4.4932	1.3618	347.976	4.9931	1.3651
347.977	5.4930	1.3683	347.970	5.9927	1.3715	347.975	6.4927	1.3746
352.861	0.6943	1.3143	352.863	0.9943	1.3171	352.860	1.4943	1.3216
352.871	1.9941	1.3259	352.868	2.4939	1.3301	352.864	2.9937	1.3342
352.866	3.4936	1.3381	352.864	3.9934	1.3419	352.865	4.4931	1.3456
352.865	4.9930	1.3492	352.865	5.4929	1.3527	352.868	5.9927	1.3560
352.865	6.4925	1.3594	357.750	0.6942	1.2950	357.739	0.9943	1.2981
357.748	1.4943	1.3030	357.743	1.9942	1.3078	357.755	2.4940	1.3123
357.756	2.9938	1.3167	357.757	3.4935	1.3210	357.759	3.9933	1.3251
357.758	4.4931	1.3290	357.762	4.9931	1.3329	357.756	5.4930	1.3367
357.749	5.9926	1.3403	357.749	6.4923	1.3439	362.577	0.7942	1.2762
362.577	0.9941	1.2784	362.579	1.4941	1.2839	362.580	1.9940	1.2892
362.585	2.4938	1.2942	362.588	2.9937	1.2989	362.595	3.4935	1.3036
362.599	3.9933	1.3080	362.593	4.4930	1.3123	362.585	4.9929	1.3165
362.596	5.4927	1.3205	362.591	5.9926	1.3244	362.588	6.4923	1.3282
367.448	0.8940	1.2565	367.428	0.9943	1.2578	367.454	1.4941	1.2639
367.453	1.9939	1.2697	367.454	2.4936	1.2752	267.456	2.9935	1.2805
367.446	3.4933	1.2856	367.440	3.9931	1.2905	367.436	4.4927	1.2952
367.435	4.9928	1.2997	367.451	5.4924	1.3040	367.447	5.9921	1.3082
367.444	6.4921	1.3123	371.579	0.9939	1.2393	371.579	1.4939	1.2461
371.578	1.9939	1.2525	371.552	2.4937	1.2587	371.553	2.9935	1.2644
371.503	3.4936	1.2700	371.500	3.9934	1.2753	371.515	4.4933	1.2803
371.498	4.9932	1.2852	371.499	5.4930	1.2898	371.492	5.9926	1.2943
371.501	6.4922	1.2986						

The deviations of the measured densities from eq 10 are shown in Figure 2. The fractional root mean square (rms) deviation is 0.006% of the density. Coefficients for eq 10 are listed in Table 6.

Saturated Liquid Density. Saturated liquid densities were calculated by evaluating eq 10 at vapor pressures determined from eq 9 on the isotherms where the compressed liquid densities had been measured. The extrapolation of eq 10 to the vapor pressure is very short; thus, it makes a negligible contribution to the uncertainty of the results. The saturated liquid densities were correlated with the function used by Pentermann and Wagner (1978):

$$\rho/\mathrm{g\cdot cm^{-3}} = B_1 + B_2\tau^{1/3} + B_3\tau^{2/3} + B_4\tau + B_5\tau^{4/3} \quad (11)$$

$B_1 = 0.5724$ $\quad T_c = 431.95$ K
$B_2 = 0.186\ 501\ 40$
$B_3 = 4.660\ 901\ 5$
$B_4 = -6.920\ 808\ 8$
$B_5 = 3.841\ 203\ 7$

where $\tau = (1 - T/T_c)$. In eq 11, the coefficient B_1 was fixed

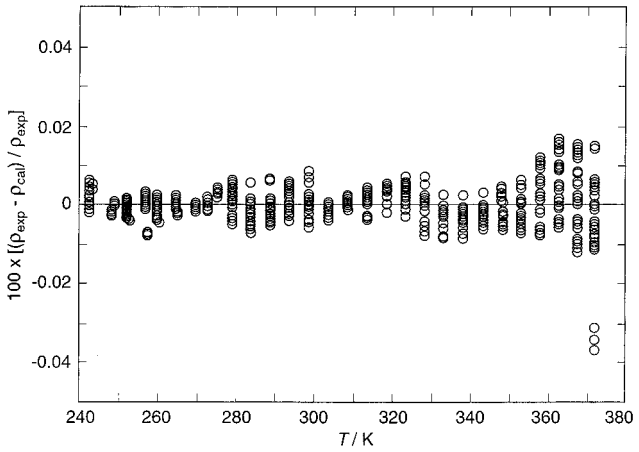

Figure 2. Compressed liquid density deviation from eq 10.

Table 6. Coefficients for Eq 10, Compressed Liquid Density Correlation

i	A_{pi}	B_{pi}	C_{pi}
1	1.565468	2.9442624×10^{-6}	$-2.8039201 \times 10^{-11}$
2	$-2.7926662 \times 10^{-3}$	3.7078983×10^{-8}	$-7.1753893 \times 10^{-13}$
3	$-2.8397851 \times 10^{-6}$	$2.3396946 \times 10^{-10}$	$-5.8421857 \times 10^{-15}$
4	$-1.1686035 \times 10^{-8}$	$-1.0827582 \times 10^{-12}$	$8.2978352 \times 10^{-17}$
5	$-2.7355820 \times 10^{-10}$	$6.6571802 \times 10^{-14}$	$-4.1058847 \times 10^{-18}$

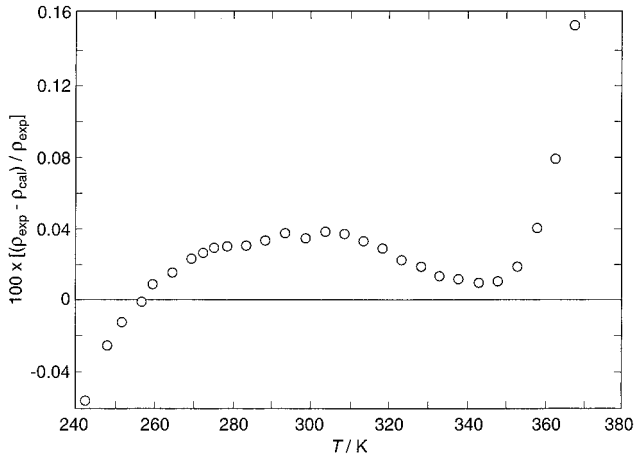

Figure 3. Saturated liquid density deviation from eq 11.

at the critical density determined from the refractive index data. Equation 11 represents the saturated liquid densities with a standard deviation of 0.06%. The deviations of the saturated liquid densities from eq 11 are shown in Figure 3.

Speed of Sound. The speed of sound $u(P,T)$ in the vapor phase of HFC-338mccq was measured at 82 state points along six isotherms over the ranges 40 kPa $\leq P \leq$ 420 kPa and 300 K $\leq T \leq$ 400 K. Table 7 provides the speed-of-sound data at each pressure−temperature state. The speed of sound was deduced from the frequencies of three resonance modes: the third and fourth longitudinal modes and first radial mode. The tabulated uncertainty ($\sigma[u]/u$) is the fractional root mean square deviation of these three measurements.

The density virial equation of state was used to analyze the sound speed results and to determine the density virial coefficients and the ideal gas heat capacity $C_p^\circ(T)$. The virial equation of state is given by

$$P = RT\rho[1 + B(T)\rho + C(T)\rho^2 + ...] \qquad (12)$$

Because only a small volume of sample was available, the pressure range was limited and eq 12 was truncated after the third virial coefficient $C(T)$. To relate the speed of sound to the virial equation of state, we used the thermodynamic relation $u^2 = (\partial P/\partial\rho)_S$ following the procedures of Gillis and Moldover (1996). We used the expansion similar to eq 12 for the speed of sound in terms of the pressure:

$$u^2 = \left(\frac{\gamma^\circ(T)RT}{m}\right)\left(1 + \frac{\beta_a(T)}{RT}P + \frac{\gamma_a(T)}{RT}P^2 + ...\right) \qquad (13)$$

where $\gamma^\circ(T) = C_p^\circ(T)/(C_p^\circ(T) - R)$, R is the universal gas constant, $m = 0.202\,047$ kg·mol^{-1} is the molar mass, and $\beta_a(T)$ and $\gamma_a(T)$ are the second and third acoustical virial coefficients, respectively. The ideal gas heat capacity was determined from eq 13 using the data for which $P \leq 120$ kPa. Its temperature dependence was represented with the polynomial function of temperature.

$$\frac{C_p^\circ(T)}{R} = 1.42658 + 0.132760T/\text{K} - 3.74658 \times 10^{-4}(T/\text{K})^2 + 4.523202 \times 10^{-7}(T/\text{K})^3 \qquad (14)$$

If the molar mass of the sample were known, the uncer-

Table 7. Speed of Sound Measurements in HFC-338mccq

P/kPa	u/m·s^{-1}	$\sigma[u]/u$	P/kPa	u/m·s^{-1}	$\sigma[u]/u$
		$T = 300.0$ K			
79.79	110.042	73.3	50.05	111.602	91.4
69.31	110.604	83.8	39.73	112.120	102.7
60.14	111.084	101.1	30.44	112.582	94.7
		$T = 320.0$ K			
181.81	109.851	88.2	80.32	114.444	71.1
162.40	110.786	85.5	69.26	114.909	74.4
141.05	111.777	77.2	59.61	115.310	92.2
122.14	112.631	75.9	51.33	115.648	85.9
102.01	113.515	72.4	40.22	116.097	82.0
		$T = 340.0$ K			
194.10	114.442	63.4	103.41	117.744	59.8
171.37	115.294	81.9	86.70	118.323	57.1
156.37	115.850	65.1	68.94	118.930	70.0
138.56	116.498	64.5	50.78	119.539	52.9
119.74	117.169	66.5			
		$T = 360.0$ K			
255.60	117.131	63.0	153.53	120.276	80.4
255.50	117.136	61.6	139.03	120.704	51.7
255.25	117.141	165.3	125.85	121.089	52.8
255.05	117.148	38.9	114.14	121.428	45.6
255.01	117.152	56.5	100.27	121.827	48.3
244.75	117.479	88.0	90.94	122.094	53.3
221.56	118.208	173.5	78.11	122.458	29.8
195.97	118.997	167.2	67.02	122.771	53.8
181.59	119.434	48.9	52.92	123.166	70.1
163.05	119.993	59.2	39.92	123.524	68.9
		$T = 380.0$ K			
263.29	121.495	50.5	137.27	124.670	59.7
263.20	121.500	49.7	127.14	124.917	41.6
263.16	121.501	51.2	114.71	125.216	37.8
263.11	121.502	48.6	100.08	125.568	38.9
245.30	121.965	96.9	90.30	125.802	39.8
202.02	123.066	58.0	78.84	126.075	35.0
164.35	124.006	44.4	67.14	126.352	40.1
152.27	124.303	50.1	54.00	126.660	53.0
		$T = 400.0$ K			
416.16	122.321	54.6	141.66	128.282	101.9
416.08	122.320	31.3	123.45	128.648	56.9
356.61	123.668	50.8	113.50	128.853	53.0
326.41	124.339	91.9	100.23	129.121	38.1
288.20	125.181	66.7	89.33	129.342	34.2
261.25	125.763	64.1	79.64	129.536	37.6
241.83	126.180	76.1	71.03	129.709	17.7
223.81	126.563	73.9	59.44	129.942	20.5
200.98	127.044	77.2	49.80	130.132	20.3
181.10	127.461	73.1	40.31	130.329	33.1
163.24	127.831	65.8			

Table 8. Parameters for the Density Virial Coefficients[a]

	$B(T)$ ($m^3 \cdot mol^{-1}$)	$C(T)$ ($m^3 \cdot mol^{-1})^2$
b_o ($m^3 \cdot mol^{-1}$)	2.739703×10^{-4}	3.886700×10^{-4}
λ	1.299 79	1.108 04
ϵ/k_B	504.87	788.45

[a] b_o is the hard-core molar volume, λ is the ratio of the width of the well to the width of the hard core, ϵ is the well depth, and k_B is Boltzmann's constant.

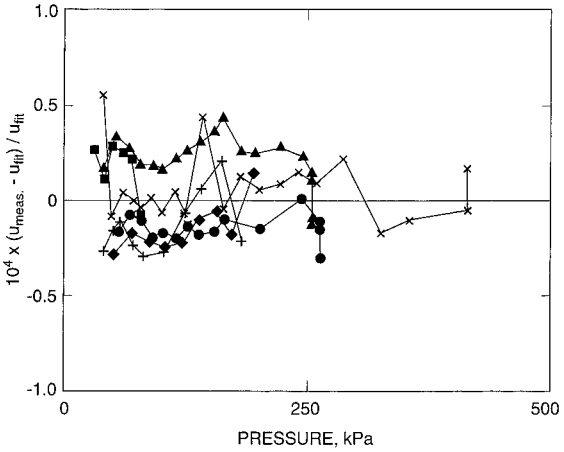

Figure 4. Deviations of the speed of sound data from fit to eq 13. Isotherms: (■) 300 K; (◆) 310 K; (+) 320 K; (▲) 360 K; (●) 380 K; (×) 400 K.

tainty in $C_p^\circ(T)$ as determined by sound speed measurements would have been on the order of 0.1%. However, the value used for m does not account for the impurities of unknown composition. Analytical examination of the sample fluid showed that the sample was only 99.7% pure. The small concentration of impurities leads to an uncertainty in the average molecular weight of the sample fluid which must be considered when deducing $C_p^\circ(T)$ from the zero pressure intercept of eq 13. We estimate that the uncertainty in the deduced value of $C_p^\circ(T)$ may be as much as 0.5% because of the impurities within the sample.

The temperature dependence of the density virial coefficients $B(T)$ and $C(T)$ was assumed to be that of the square-well intermolecular potential model, as given in eqs 15 and 16.

$$B(T) = b_0[1 - (\lambda^3 - 1)\Delta] \tag{15}$$

$$C(T) = \frac{1}{8}b_0^2(5 - c_1\Delta - c_2\Delta^2 - c_3\Delta^3) \tag{16}$$

$$c_1 = \lambda^6 - 18\lambda^4 + 32\lambda^3 - 15$$
$$c_2 = 2\lambda^6 - 36\lambda^4 + 32\lambda^3 + 18\lambda^2 - 16$$
$$c_3 = 6\lambda^6 - 18\lambda^4 + 18\lambda^2 - 6$$

where

$$\Delta = e^{\epsilon/k_B T} - 1$$

A nonlinear fitting algorithm was then employed to fit eq 13 to the $u(P,T)$ data (Gillis and Moldover (1996)), resulting in the parameters for the density virial coefficients listed in Table 8. The fit of all 82 points had 73 degrees of freedom and resulted in a fit with a χ^2 of 11.34 and a fractional rms deviation of only 0.002% of the speed of sound. The deviations of the measured speeds of sound from the fit are given in Figure 4. Note that all but one state point are within ±0.005% of the base line.

Critical Density. As mentioned in the text following eq 5, the refractive index data lead to the value $\rho_c = 572.4$ ± 3.0 $kg \cdot m^{-3}$, where the uncertainty was estimated from fitting the densities deduced from the Lorentz−Lorenz relation. From the present data we can estimate the critical density without using the Lorentz−Lorenz relation. We have done so using the "law of the rectilinear diameter", as shown in Figure 5. For this estimate we used the values of ρ_l obtained from the present densimeter data together with values of ρ_v obtained from evaluating the virial equation (eq 12) at the vapor pressure (eq 10) on up to 373 K. The values of the virial coefficients were obtained from the speed-of-sound data. This procedure leads to the value $\rho_c = 572.0$ $kg \cdot m^{-3}$ which is only 0.07% smaller than the value deduced from the refractive index data.

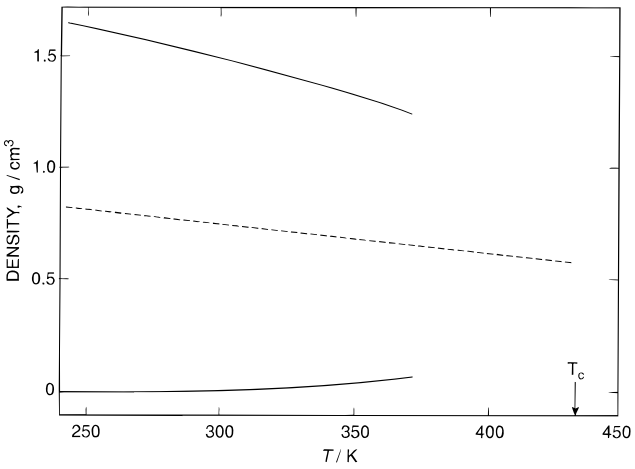

Figure 5. Rectilinear diameter to determine the critical density of HFC-338mccq from saturated liquid densities and saturated vapor densities from the column labeled "acoustic" in Table 9.

We obtained yet another value for the critical density, ($\rho_c = 571.5$ $kg \cdot m^{-3}$, by using Weber's correlation to estimate the virial coefficients and ρ_v; see next section. The spread among the three values of ρ_c is only 0.9 $kg \cdot m^{-3}$, suggesting that the error estimate cited (±3.0 $kg \cdot m^{-3}$) is quite conservative.

Alternative Estimate of Vapor Density. In Table 9, the saturated vapor densities obtained from three sources are compared. The densities in the columns labeled "acoustic" and "estimate" result from extrapolating the virial equation of state to the vapor pressure curve. For the "acoustic" column, the virial coefficients were obtained from the square-well model for the speed-of-sound data. For the "estimate" column, we used the correlation of Weber (1994). Weber utilized "universal" functions and the substance specific critical parameters; T_c, P_c, V_c, the acentric factor ω, and the dipole moment μ. To apply Weber's method, we used the present value of T_c and the value of P_c obtained by extrapolating the vapor pressure data to T_c. The refractive index data yielded the value $1/V_c$. The acentric factor, $\omega = 0.4129$, was found from eq 10. (The acentric factor is defined as $\omega = -\log(P^\Phi/P_c) - 1$, where P^Φ is the vapor pressure at $0.7T_c$). The dipole moment μ = 1.866 D was recently measured (Mehl (1996)).

We have tested the accuracy of Weber's method in previous publications (Defibaugh et al. (1996)) with other fluids for which gas-phase PVT data have been published. We have also compared Weber's predicted virials, $B(T)$ and $C(T)$, with the virials determined by the speed of sound. The comparisons led us to the conclusion that the estimated saturated vapor densities have a worst-case uncertainty on the order of 2% when $T/T_c < 0.9$; however, this method has not been tested with butane-based molecules. Table 9 shows that below 370 K, the acoustic and estimated ρ, agree within 0.12%. At 400 K, the highest temperature of

Table 9. Saturated Vapor Densities for HFC-338mccq

		ρ/mol·L^{-1}		
T/K	P/kPa	acoustic	estimate	refractive index
240	4.94	0.0025	0.0025	
245	6.80	0.0034	0.0034	
250	9.23	0.0045	0.0045	
255	12.34	0.0059	0.0059	
260	16.26	0.0076	0.0076	
265	21.16	0.0098	0.0098	
270	27.20	0.0124	0.0124	
275	34.56	0.0155	0.0155	
280	43.46	0.0192	0.0192	
285	54.10	0.0236	0.0236	
290	66.74	0.0288	0.0287	
295	81.61	0.0348	0.0348	
300	98.98	0.0418	0.0417	
305	119.14	0.0498	0.0498	
310	142.37	0.0590	0.0590	
315	168.98	0.0696	0.0696	
320	199.29	0.0816	0.0815	
325	233.64	0.0952	0.0951	
330	272.36	0.1105	0.1105	0.1127
335	315.81	0.1278	0.1278	0.1273
340	364.36	0.1473	0.1472	0.1445
345	418.39	0.1691	0.1691	0.1646
350	478.27	0.1936	0.1936	0.1878
355	544.43	0.2210	0.2211	0.2143
360	617.26	0.2518	0.2519	0.2445
365	697.21	0.2862	0.2864	0.2787
370	784.72	0.3248	0.3252	0.3175
375	880.25	0.3682	0.3689	0.3613
380	984.30	0.4172	0.4183	0.4109
385	1097.36	0.4727	0.4743	0.4670
390	1219.99	0.5359	0.5383	0.5309
395	1352.76	0.6087	0.6123	0.6039
400	1496.30	0.6937	0.6989	0.6881
405	1651.30		0.8026	0.7863
410	1818.52		0.9317	0.9028
415	1998.87		1.1057	1.0449
420	2193.38			1.2261
425	2403.44			1.4784
430	2631.11			1.9359
431.95	2725.70			2.8331

the speed-of-sound data, the acoustic and estimated ρ_v differ by only 0.74%.

CSD Equation of State. We deduced the coefficients for the Carnahan−Starling−DeSantis (CSD) equation of state (Carnahan and Starlings (1972), DeSantis et al. (1976) to describe approximately the thermodynamic properties of HFC-338mccq over the temperature range 243 K to 373 K. The Carnahan−Starling−DeSantis (CSD) equation of state is

$$\frac{pV}{RT} = \frac{1 + y + y^2 - y^3}{(1-y)^3} - \frac{a}{RT(V+b)} \qquad (17)$$

where

$$y = \frac{b}{4V}$$

For HFC-338mccq, the coefficients a and b have the temperature-dependent representation:

$$a/\mathrm{kJ{\cdot}m^3{\cdot}kg^{-1}{\cdot}mol^{-2}} = 7959.2798 \exp(-2.3703526 \times 10^{-3} T/\mathrm{K} - 1.8005537 \times 10^{-6} (T/\mathrm{K})^2) \qquad (18)$$

$$b/\mathrm{m^3{\cdot}kg^{-1}{\cdot}mol^{-1}} = 0.24958393 - 1.9263272 \times 10^{-4} T/\mathrm{K} - 2.2163593 \times 10^{-7} (T/\mathrm{K})^2 \qquad (19)$$

Here T is in kelvin and $R = 8.314\,471$ J·mol^{-1}·K^{-1} is the universal gas constant.

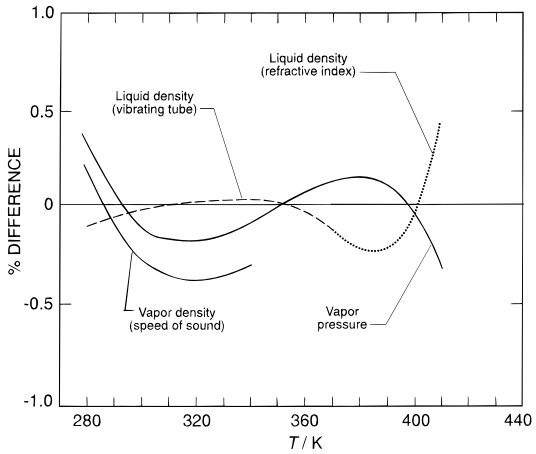

Figure 6. Deviations from the CSD equation of state of the vapor pressure and the saturated liquid and vapor densities.

The parameters for the CSD equation were chosen to reproduce approximately the vapor pressures and the saturated liquid densities that we measured as well as the estimates of the saturated vapor densities. Figure 6 shows the deviations of these saturation properties from the CSD equation of state. The CSD equation reproduces the experimental saturation properties of HFC-338mccq to within ±0.4% throughout the temperature range of 280 K to 410 K except for the saturated vapor densities above 340 K.

It is well-known that the CSD equation does not represent the critical region adequately. In the critical region, the saturated liquid and vapor densities can be determined from eqs 4 and 5.

From the data obtained in this work, the critical parameters for HFC-338mccq are estimated to be

$$T_c = (431.95 \pm 0.02)\ \mathrm{K}$$

$$P_c = (2725 \pm 15)\ \mathrm{kPa}$$

$$\rho_c = (572.4 \pm 3.0)\ \mathrm{kg{\cdot}m^{-3}}$$

We recall that these estimates do not account for the impurities in the sample. These impurities are likely to be chemically similar to the HFC-338mccq and comprise approximately 0.3% of the sample.

Acknowledgment

We thank John Gallagher for his assistance with software development and also Keith Gillis with helpful discussions concerning the speed of sound measurements.

Literature Cited

Carnahan, N. F.; Starling, K. E. Intermolecular Repulsions and Equation of State for Fluids. *AIChE J.* **1972**, *18*, 1184−1189.

Chae, H. B.; Schmidt, J. W.; Moldover, M. R. Alternative refrigerants R123, R134, R141b, R142b, and R152a: critical temperature, refractive index, surface tension and estimates of liquid, vapor and critical densities. *J. Phys. Chem.* **1990**, *94*, 8840−8845.

Defibaugh, D. R.; Morrison, G. Compressed liquid densities and saturation densities of chlorodifluoromethane. *J. Chem. Eng. Data* **1990**, *37*, 107−110.

Defibaugh, R. D.; Moldover, M. R. Compressed and Saturated Liquid Densities for 18 Halogenated Organic Compounds. *J. Chem. Eng. Data* **1997**, *42*, 160−168.

Defibaugh, D. R.; Gillis, K. A.; Moldover, M. R.; Schmidt, J. W.; Weber, L. A. Thermodynamic Properties of 1,1,1,2,3,3-hexafluoropropane. *Fluid Phase Equilib.* **1996**, *122*, 131−155.

DeSantis, R.; Gironi, F.; Marrelli, L. Vapor-Liquid Equilibrium from a Hard-sphere Equation of State. *Ind. Eng. Chem. Fundam.* **1976**, *15*, 183−189.

Gillis, K. A. Thermodynamic properties of two gaseous halogenated ethers from speed of sound measurements: difluoromethoxy-difluoromethane and 2-difluoromethoxy-1,1,1-trifluoroethane. *Int. J. Thermophys.* **1994**, *15*, 821.

Gillis, K. A.; Moldover, M. R. Practical determination of gas densities from the speed of sound using square-well potentials. *Int. J. Thermophys.* **1996**, *17*, 1305.

Gillis, K. A.; Goodwin, A. R. H.; Moldover, M. R. Accurate acoustic measurements in gases under difficult conditions. *Rev. Sci. Instrum.* **1991**, *62*, 2213.

Goodwin, A. R. H.; Defibaugh, D. R.; Weber, L. A. The vapor pressure of 1,1,1,2-tetrafluoroethane (R134a) and chlorodifluoromethane (R22). *Int. J. Thermophys.* **1992a**, *13*, 837−854.

Goodwin, A. R. H.; Defibaugh, D. R.; Morrison, G.; Weber, L. A. The vapor pressure of 1,1-dichloro-2,2,2-trifluoroethane (R123). *Int. J. Thermophys.* **1992b**, *13*, 999−1008.

Lane, J. E. Correction terms for calculating surface tension from capillary rise. *J. Colloid Interface Sci.* **1973**, *42*, 145.

Mehl, J. B.; Goodwin, A. R. H. Measurement of the Dipole Moments of Seven Partially Fluorinated Hydrocarbons with a Radio-Frequency Reentrant Cavity Resonator. *Int. J. Thermophys.* **1996**, *18*, No. 3.

Montreal Protocol on Substances that Deplete the Ozone layer; Final Act, United Nations Environmental Program (UNEP), Sept 16, 1987.

Pentermann, W.; Wagner, W. New pressure-density-temperature measurements and new rational equation for the saturated liquid and vapor densities of oxygen. *J. Chem. Thermodyn.* **1978**, *10*, 1161−1172.

Weber, L. A. Ebulliometric measurements of the vapor pressures of R123 and R141b. *Fluid Phase Equilib.* **1992**, *80*, 141.

Weber, L. A. Estimating the virial coefficients of small polar molecules. *Int. J. Thermophys.* **1994**, *15*, 461−482.

Weber, L. A.; Goodwin, A. R. H. J. Ebulliometric measurements of the vapor pressures of difluoromethane. *J. Chem. Eng. Data* **1993**, *38*, 254.

Received for review September 23, 1996. Accepted January 16, 1997.[⊗] This work was supported in part by the Environmental Protection Agency under interagency agreement DW13935432-01-4. The development of many of the apparatus used to perform this work was supported in part by the Division of Engineering and Geosciences, Office of Basic Energy Sciences, U.S. Department of Energy.

JE9603133

[⊗] Abstract published in *Advance ACS Abstracts*, March 1, 1997.